Research Square

Preprints are preliminary reports that have not undergone peer review.
They should not be considered conclusive, used to inform clinical practice,
or referenced by the media as validated information.

Exploring the Influence of Cortical Microstructural Diffusion on Functional Brain Networks

Yating Wu
Northern Jiangsu People's Hospital
Xue Wang
Graduate School of Dalian Medical University
Song'an Shang
Northern Jiangsu People's Hospital
Jing Ye
Northern Jiangsu People's Hospital
Jacob Xiang
Clinical Pharmacist, Foothills Medical Centre
Xiang Lv
Northern Jiangsu People's Hospital
Yao Xu
Northern Jiangsu People's Hospital
Hongying Zhang
zhying11@aliyun.com

Northern Jiangsu People's Hospital

Research Article

Keywords: Diffusion Kurtosis Imaging, Brain Functional Networks, Microstructure Characteristics, Cortex, Resting State Functional Magnetic Resonance Imaging

Posted Date: March 10th, 2026

DOI: https://doi.org/10.21203/rs.3.rs-8849836/v1

License: This work is licensed under a Creative Commons Attribution 4.0 International License.
Read Full License

Additional Declarations: No competing interests reported.

Abstract

Objective

The cortex is the primary source of blood-oxygenation-level dependent (BOLD) signals, and it is often believed that the brain structural modules serve as the cornerstones of the functional networks. Although a great deal of work had been done in the past to map the white matter fiber connections among various cortical regions in order to clarify the functional connectivity, it is still unclear how the diffusion property of the inner cortex's microstructure relates to the functional brain networks. This study aims to investigate the connection between the canonical brain functional networks and the complexity of cortical microstructural diffusion.

Methods

Kurtosis diffusion (DK) and resting state functional MRI data from 30 healthy volunteers were collected. The group level networks of default mode network (DMN), executive control network (ECN), dorsal attention network (DAN), salience network (SN), sensorimotor network (SMN) and visual network (VN) were extracted, and network masks were made on the T1 gray matter images after segmentation. Then, the diffusion parameter maps with kurtosis and tensor properties were calculated from the DK data, and co-registrated with the cortical T1 images. These diffusion kurtosis parameters of AK, RK, MK, KFA, and tensor parameters of AD, RD, MD, FA values in each individual were extracted based on each of the function network mask. The diffusion parameter values of above networks were analyzed by ANOVA method of non-parametric test.

Results

Statistical analysis showed that the values of AK, RK, MK and KFA in low-order networks (SMN, VN) were significantly higher than those in high-order networks (DMN, ECN, DAN and SN), and no significant differences were observed within either the low-order or high-order networks respectively. The values of RD in SN were significantly lower than those in VN and SMN. The values of FA in SN and ECN were significantly lower than those in SMN.

Conclusions

Our knowledge of the foundations of brain networks has advanced as a result of the findings, which suggested that the kurtosis diffusion of microstructure within the human cerebral cortex is topologically distributed and corresponds to the hierarchy between low-order and high-order functional networks. The DKI-specific diffusion model is suitable for mapping the networks of structural inner cortices.

1. Introduction

Execution, goal direction, control, information recognition, and tactile processing are among the many human tasks that depend on the dynamic activity and collaboration of brain neurons for survival. Brain communications could be investigated using a variety of methods, including electroencephalograms (EEG), functional near-infrared spectroscopy (fNIRS), and resting-state functional magnetic resonance imaging (rs-fMRI) that is dependent on blood oxygenation level (BOLD)[1–3]. BOLD rs-fMRI has been particularly useful in identifying large-scale brain functional networks, such as the default mode network (DMN), executive control network (ECN), dorsal attention network (DAN), salience network (SN), sensorimotor network (SMN), and visual network (VN), by measuring synchronized hemodynamic changes associated with neuronal activity[1–5].This method offers a respectable temporal and spatial resolution. Functional connectivity measurements have been used in numerous researches to successfully identify the key cortical regions within functional networks.

However, the precise process by which brain networks operate is still unknown. It is well acknowledged that the basis for sustaining and facilitating functional communications is provided by brain structures. Whole-brain segmentation has been supported by postmortem examination, which has shown unique patterns of cortical cytologic organization in specific brain areas. One such region is Brodmann's area, which has been closely linked to functional specialization[6, 7]. Moreover, variations in neuron and total cell densities across different functional areas on the cortical layer had been reported, with differences of up to fivefold[8]. In vivo studies had also demonstrated that cortical thickness, gray matter (GM) volumes, and the extent of cortical folding exhibit covariance with the different functional brain regions[9–11]. These findings make one wonder if more research should be done on the internal characteristics of the cortex at the level of the structural foundation of brain networks in the physiological state, going beyond conventional morpho-volumetry.

Network theory provides a valuable framework for modeling the coupling between structure and function in neurobiological systems, spanning different species and spatial scales[12]. Reliable structure-function connections had been shown in recent research at the whole-brain, global, and regional levels; this coupling can change in older persons experiencing cognitive decline[13–15]. Investigations have also shown significant variation in the strength of the regional structure-function coupling throughout the cortex, with primary sensory-motor areas showing higher laminar structure-function coupling and white matter fiber bundle connectivity-function coupling in the cortex, which is consistent with the brain's functional specialization[16]. Previous studies had primarily utilized multiple computational models, including network diffusion models, graph theoretical approaches, and structural covariance patterns, to elucidate functional connectivity based on the measures of white matter diffusion, cortical expansion, and thickness[14, 17–21]. However, it is important to note that the structural-functional specificity cannot be solely attributed to white matter diffusion and T1 structure properties; equal attention should be given to the diffusion properties within the cortical GM.

The brain's white matter (WM) fibers may be efficiently observed and tracked in both healthy and diseased states using diffusion tensor imaging (DTI) technology, which is extremely sensitive to WM tissues that follow Gaussian distributions. In light of the assumption that there are direct WM fiber connections between distinct functional network nodes, previous studies had revealed only a limited number of WM fiber tracts that can account for functional connectivity[22, 23]. Compared to WM, the cortical GM has a more complex structure, and has the greatest contribution to BOLD signals[24]. The GM is comprised of a multitude of neuronal cell bodies, dendrites, glial cells, synapses, and capillaries, exhibiting a relatively non-Gaussian distribution. Diffusion kurtosis imaging (DKI) is an extension of DTI, which provides kurtosis values that are more sensitive to the non-Gaussian diffusion effect of water molecules and is used to quantify the complexity of tissue structure, such as GM[25]. The DKI metrics across whole cerebral cortex demonstrated good test-retest reliability, and altered at a series of brain disease[26, 27].

At present, the influence of microstructural diffusion properties within cortex on functional brain networks remains poorly understood. Consequently, this study aims to investigate the potential correlations between the large-scale brain functional networks and their coordinative cortical microstructural diffusion characteristics. By doing so, we hope to gain a deeper insight into the underlying mechanisms of functional networks.

2. Materials and Methods

2.1 Subjects

A total of 30 healthy subjects with right-handed were recruited (mean age, 38.8 ± 4.3 years; 15 males), without previous history of neurological, psychiatric, head trauma, or cardiovascular disorders; no drug and alcohol abuse; none of the subjects showed abnormal findings in their structural brain MRIs. All the subjects had normal Minimum Mental State Examination. This study was approved by the Ethics Committee of Northern Jiangsu People's Hospital. All the subjects were fully informed of the nature and process of the study; they all provided written informed consent.

2.2 Data Acquisition

MR images were acquired at GE 3.0 T scanner (Discovery 750; GE Healthcare, Milwaukee, Wisconsin, USA), equipped with an eight-channel phased array head coil. The imaging protocol included BOLD, high resolution T1-weighted 3D brain volume (3D-T1 BRAVO), and DKI sequence. Rs-fMRI data was collected with an echo-planar imaging (EPI) sequence with parameters: TR/TE = 2000/30ms, flip angle = 90°, FOV = 240 × 240 mm2, matrix size = 64 × 64, slice thickness, 4mm without gap, number of time points = 240, scan duration = 8min. DKI data were obtained using a single-shot EPI sequence with parameters: TR/TE = 8000/92.2ms, FOV = 250 × 250 mm, matrix size = 100 × 100, slice thickness, 2.5 mm without gap. Diffusion encoding was applied with b values of 1250, and 2500 s/mm2, each with 30 diffusion directions. The scan duration was 8 min and 32 sec. The 3D-T1 images were obtained in the sagittal

plane with the following parameters: TR/TE = 8.20/3.20ms, acquisition matrix = 256 × 256, FOV = 256 mm, slice thickness = 1 mm, 176 sagittal slices, scan duration = 4 min and 2 sec.

2.3 Data preprocessing and analysis

The fMRI data preprocessing was performed using DPARSF software V2.3 (http://www.restfmri.net), which is based on SPM8 (http://www.fil.ion.ucl.ac.uk/spm) and the Resting-State fMRI Data Analysis Toolkit (Beijing Normal University, Beijing, http://www.restfmri.net). The first ten volumes were discarded. The images were corrected for slice timing and realigned for head movement correction. T1 weighted 3D images were segmented into three components of gray matter (GM), white matter, and cerebrospinal fluid. The functional images were normalized using DARTEL. Nine subjects were excluded because their head movement translation exceeded 2.5 mm or rotation exceeded 2.5° criterion. The normalized volumes were re-sampled to a voxel size of 3mm × 3mm × 3mm in MNI space, and the EPI images were spatially smoothed using an isotropic Gaussian filter (4 mm FWHM). The movement parameters (Friston 24-parameter model[28]) and signals of white matter, cerebrospinal fluid and global mean were regressed out. Linear detrending and temporal bandpass filtering (0.01– 0.08 Hz) were applied.

The subsequent data processing and statistical analyses were performed. Five canonical networks including DMN, ECN, DAN, SN, SMN and VN were extracted by using seed-based functional connectivity analysis. The seed regions of interest (ROIs) with 6mm radius spheres were created by referring to previous studies[29, 30]. The MNI coordinates of seed ROI corresponding to the resting state networks were as follows: DMN (posterior cingulate cortex, PCC/ ventral medial prefrontal cortex, vmPFC): 0, -53, 26/ 0, 52, -6; ECN (left and right dorsolateral prefrontal cortex, l/r DLPFC): -42, 34, 20/ 44, 36, 20; DAN (left and right superior parietal lobule (SPL): (-25, -53, 52/25, -57, 52); SN (left and right anterior-insular cortex, l/r AIC):-32, 26, -14/ 38, 22, -10; SMN (left and right precentral gyrus, l/r PrCG): -28, -16, 66/ 28, -16, 66; and VN (left and right V2 primary cortex:19, -95, 2/ -19, -95, 2). The seed time series in the two ROIs for each network were averaged. The positive Pearson correlation coefficients between the seed time series and the time series in other voxels in the brain were calculated. A Fisher's z-transform was applied to improve the normality of these correlation coefficients. One-sample *t* test was performed to determine group functional network corrected by False Discovery Rate (FDR), with the threshold at $p < 0.01$, cluster size > 50. Each brain network was saved as a mask and normalized to a voxel size of 2mm × 2mm × 2 mm to match the size of diffusion image space. To avoid the interference of subcortical white matter, the saved network masks were merged with each individual normalized 3D-T1 structural cortex images obtained during above preprocess segmentation. The merged individual cortical images for each canonical network were saved separately as masks for next step to extract the diffusion metric values.

All diffusion datasets preprocessing included the removal of non-brain tissue and correction of movement and eddy current distortion. Next, DKI and DTI parameters were processed using Diffusion Kurtosis Estimator (DKE) (http://www.nitrc.org/projects/dke) toolkit[31]. Tensor of diffusion (DT) and kurtosis of diffusion (DK) parameters were extracted in DKE using the CLLS-QP algorithm. These parametric maps included DTI metrics of mean diffusivity (MD), axial diffusivity (AD), radial diffusivity

(RD), fractional anisotropy (FA) and the corresponding DKI metrics of mean kurtosis (MK), axial kurtosis (AK), radial kurtosis (RK) and kurtosis fractional anisotropy (KFA). All the resultant DKI parametric maps, then, were normalized by an affine co-registration to the T1 weighted 3D anatomic images. Next, all DKI parametric maps were normalized into the MNI space using the deformation matrix created in the fMRI preprocessing step. A resolution of 2 × 2 × 2mm was finally used as voxel size.

2.4 Statistical analysis

The diffusion parameter values in each individual were extracted from each individual merged network masks obtained in above steps. The statistical analysis for DK and DT metric values across the six canonical networks was performed by the Statistical Package for the Social Sciences (SPSS, version 25.0) software (IBM, Armonk, NY, USA), with Kruskal-Wallis H test, and Bonferroni's correction with a $p < 0.05$ was used for post hoc analysis. The data processing pipeline was illustrated in Fig. 1.

3. Results

3.1. Group level of network cortical masks

Figure 2 visually demonstrates the successful acquisition of the six canonical networks, which were exclusively projected onto the cortex regions. These maps exhibit consistency with the distribution of previously identified traditional networks.

3.2. Calculation of the diffusion parameters in masks

Figure 3 displays the DK and DT metric values (mean ± standard deviation) in the cortical regions of the six canonical networks. It shows that the values of KFA and FA are much smaller than those of the other diffusion parameters obviously. It can be noted that the FA values within all the network regions were very low compared to the other parameter values.

3.3 Comparisons of DK parameters between networks

As all diffusion metric values did not follow a normal distribution, a Kruskal-Wallis H test and Bonferroni's post-hoc analysis was conducted. When comparing DMN, ECN, DAN and SN with SMN and VN individually, significant differences were observed for each of the DK metrics (AK, RK, MK, KFA) ($p < 0.05$). Specifically, the DK metric values in DMN, ECN, DAN and SN were lower than those in SMN and VN, whereas no significant difference was detected when comparing DMN, ECN, and SN among themselves, nor is there any significant dissimilarity between SMN and VN ($p > 0.05$). The detailed p-values are shown in Fig. 4 as a 6×6 matrix diagram.

3.4 Comparisons of DT parameters between networks

As all diffusion metric values did not follow a normal distribution, a Kruskal-Wallis H test and Bonferroni's post-hoc analysis was conducted. When comparing DMN, ECN, DAN and SN with SMN and VN individually, it is showed that the value of RD in SN was significantly lower than those in VN and SMN.

And the value of FA in SN and ECN was significantly lower than those in SMN. The detailed *p*-values are shown in Fig. 5 as a 6×6 matrix diagram.

4. Discussion

In this study, we investigated the microstructural diffusion properties within the cortex regions of the canonical functional networks. These six functional networks can be classified into high-order networks (DMN, ECN, DAN and SN) and low-order networks (SMN, VN) based on their associations with cognitive function[32, 33]. Our findings revealed distinct diffusion characteristics in the cortex between high-order and low-order networks, as well as convergent characteristics within each group. This provided insight into the specialization of cortical architectural organization between high-order and low-order networks at mesoscopic scale.

We propose that the differences in diffusion parameters between high-order and low-order networks could be attributed to their micro-anatomical distinctions. According to the myeloarchitectonic map of the entire human brain, primary sensory and motor regions had higher neuronal densities and densities of myelinated structures than other cortical areas [34], and the primary sensory cortices exhibited heterotypical koniocortex characteristics distinct from the homotypical cortex under microscope[35, 36]. In vivo ultra-high field MRI T_2* mapping studies also demonstrated of lower values in these primary cortices, which reflect a higher degree of myelin content[37]. The increased presence of cell membranes, organelles, and complex micro-environments within these regions further impedes the diffusion of water molecules, which can be precisely quantified by a series kurtosis metrics[38, 39]. The magnitude of the K-value and the degree of diffusion obstruction are proportional to the complexity of the tissue being imaged[40, 41]. As demonstrated in our finding that higher kurtosis metric values in low-order networks contrast with those in the high-order networks, it could be explained by the fact that there are more diffusion hindrances caused by more complex micro-architectures in the low-order network cortex. Specially, the MK has been previously demonstrated to monitor alterations in the level of myelination and is regarded as a more distinctive indicator of the microstructure of tissues[42, 43]. Another previous experiment using the monkey brain had found a direct correlation between MK values and histological images, and similar to our findings, MK values were significantly higher in low-order network cortices than those in high-order network cortices[44]. In addition, the more complex microstructure of the primary sensorimotor system implies an increased restriction of cortical structure to function, which could enhance the specialization of sensorimotor system networks.

It should be noted, however, that our results do not exactly imply that the microstructure of high-order networks are less complex than that of low order networks. High order network cortices are the regions of elevated metabolic activity with a greater abundance of cerebral blood flow. These cortical high blood flow makes them susceptible to capillary pulse movements, which could increase the apparent diffusion coefficient and lower the diffusion kurtosis parameters' value [45]. The DKI metrics only reflect the complexity of the cortical microstructure form the aspect of diffusion property.

Our results also suggest that there are convergent features in the microstructural diffusion of high-order and low-order networks respectively. The DMN is considered the core of the brain's networks, displaying heightened metabolic activity during periods of rest, while also exhibiting temporospatial anti-correlations with the DAN or ECN in response to a range of cognitive tasks[46, 47]. Additionally, the ECN and DMN often exhibit high activation together in cognitive processes involving the modulation of top-down, self-generated information[48, 49].The SN plays a dynamic switching role between the DMN and ECN[50, 51]. Hence, it is hypothesized that this convergence in microstructural diffusion within these high-order networks could ensure and facilitate their flexible integration and disintegration during advanced cognitive functions. There is a tight connection among the sensorimotor regions, as evidenced by the fact that the primary visual cortex and sensorimotor areas develop earlier and quicker than the higher-order network regions[52]. Moreover, sensory and motor areas tend to have more clustered short-range connections[53, 54]. In particular, visual stimuli frequently often do not necessitate intricate serial reprocessing and are most easily recognized where the motor cortex drives inputs[55]. Given these considerations, it seems reasonable to posit that the convergent diffusion properties within these primary cortices likely promote tight coordination between sensorimotor and visual functions, facilitating an instinctive response to external stimuli.

Due to the isotropic nature of GM and its comparatively low FA value, the sensitivity of DTI to variations in GM structure is constrained [56]. As for our findings of DT parameters, differences were observed only between SMN and individual high-order brain networks in RD and FA values. DT parameters appeared to be less sensitive than the DKI parameters in reflecting network hierarchy. To some extent, this finding reflects the limitations of DTI in detecting the complexity of gray matter microstructure.

5. Limitations

Several limitations must be acknowledged in the present study. Firstly, our data were obtained from a relatively small sample of adults, which may limit the generalizability of our findings. Secondly, our findings need multicenter study and reliability test. Thirdly, it is required to verify the sensitivity of the connection between cortical kurtosis diffusion and functional network at brain disease state.

6. Conclusion

In summary, our study provided valuable insights into the potential mechanism of cortical functional networks by investigating their regional inner cortex diffusion kurtosis characteristics. The intrinsic cortical microstructural diffusion exhibited topological organizations corresponding to the hierarchal high-order and low-order brain networks. These findings contribute to our understanding of the structure-function relationships among brain networks.

Declarations

Ethical standards

This study has been approved by the Medical Ethics Committee of Northern Jiangsu People's Hospital. All procedures performed in the studies involving human participants were in accordance with the ethical standards of the institutional and/or national research committee and with the 1964 Helsinki Declaration and its later amendments or comparable ethical standards.

Informed consent

Informed consent has been taken from parents/legal guardians of the participants of the study.

Funding

This work was supported by the Key R&D Program of Yangzhou city (YZ2021089), National Natural Science Foundation of China (82202120), Science and Technology Project of Yangzhou (YZ2022071, YZ2023082), Medical Research Program of Jiangsu Health Commission (M2022059), Clinical research project of Clinical Medical College, Yangzhou University (SBLC22004).

Author Contributions

Conceptualization, H.-Y.Z. and Y.-T.W.; methodology, Y.-T.W., S.S., J.Y., X.L., Y.X. and H.-Y.Z.; software Y.-T.W., X.W., S.S., J.Y., Jacob Xiang, X.L., Y.X. and H.-Y.Z.; validation, Y.-T.W., X.W. and H.-Y.Z.; formal analysis, Y.-T.W.; investigation, Y.-T.W., X.W., S.S., J.Y., X.L., Y.X. and H.-Y.Z.; resources, Y.-T.W., X.W. and H.-Y.Z.; data curation, Y.-T.W., X.W., S.S., J.Y., X.L., Y.X.; writing—original draft preparation, Y.-T.W. and H.-Y.Z.; writing—review and editing, S.S. and H.-Y.Z.; visualization, Y.-T.W. and H.-Y.Z.; supervision, S.S., J.Y., X.L., Y.X. and H.-Y.Z.; project administration, S.S., J.Y., X.L., Y.X. and H.-Y.Z. All authors have read and agreed to the published version of the manuscript.

References

1. Axmacher N, Mormann F, Fernández G, Elger CE, Fell J (2006) Memory formation by neuronal synchronization. Brain Res Rev 52(1):170–182. https://doi.org/10.1016/j.brainresrev.2006.01.007
2. Van Dijk KR, Hedden T, Venkataraman A, Evans KC, Lazar SW, Buckner RL (2010) Intrinsic functional connectivity as a tool for human connectomics: theory, properties, and optimization. J Neurophysiol 103(1):297–321. https://doi.org/10.1152/jn.00783.2009
3. Homae F, Watanabe H, Otobe T, Nakano T, Go T, Konishi Y et al (2010) Development of global cortical networks in early infancy. J neuroscience: official J Soc Neurosci 30(14):4877–4882. https://doi.org/10.1523/JNEUROSCI.5618-09.2010
4. Yeo BT, Krienen FM, Sepulcre J, Sabuncu MR, Lashkari D, Hollinshead M et al (2011) The organization of the human cerebral cortex estimated by intrinsic functional connectivity. J Neurophysiol 106(3):1125–1165. https://doi.org/10.1152/jn.00338.2011
5. Damoiseaux JS, Rombouts SA, Barkhof F, Scheltens P, Stam CJ, Smith SM et al (2006) Consistent resting-state networks across healthy subjects. Proc Natl Acad Sci USA 103(37):13848–13853. https://doi.org/10.1073/pnas.0601417103

6. Kawamura M (2017) [Korbinian Brodmann's Scientific Profile, and Academic Works]. Brain and nerve = Shinkei kenkyu no shinpo. ;69(4):301 – 12. https://doi.org/10.11477/mf.1416200746
7. Jones AR, Overly CC, Sunkin SM (2009) The Allen Brain Atlas: 5 years and beyond. Nat Rev Neurosci 10(11):821–828. .https://doi.org/10.1038/nrn2722
8. Collins CE (2011) Variability in neuron densities across the cortical sheet in primates. Brain Behav Evol 78(1):37–50. https://doi.org/10.1159/000327319
9. Valk SL, Xu T, Margulies DS, Masouleh SK, Paquola C, Goulas A et al (2020) Shaping brain structure: Genetic and phylogenetic axes of macroscale organization of cortical thickness. Sci Adv 6(39). https://doi.org/10.1126/sciadv.abb3417
10. Colibazzi T, Zhu H, Bansal R, Schultz RT, Wang Z, Peterson BS (2008) Latent volumetric structure of the human brain: Exploratory factor analysis and structural equation modeling of gray matter volumes in healthy children and adults. Hum Brain Mapp 29(11):1302–1312. https://doi.org/10.1002/hbm.20466
11. Wang Y, Leiberg K, Ludwig T, Little B, Necus JH, Winston G et al (2021) Independent components of human brain morphology. NeuroImage 226:117546. https://doi.org/10.1016/j.neuroimage.2020.117546
12. Bassett DS, Sporns O (2017) Network neuroscience. Nat Neurosci 20(3):353–364. https://doi.org/10.1038/nn.4502
13. Wang J, Khosrowabadi R, Ng KK, Hong Z, Chong JSX, Wang Y et al (2018) Alterations in Brain Network Topology and Structural-Functional Connectome Coupling Relate to Cognitive Impairment. Front Aging Neurosci 10:404. https://doi.org/10.3389/fnagi.2018.00404
14. Gu Z, Jamison KW, Sabuncu MR, Kuceyeski A (2021) Heritability and interindividual variability of regional structure-function coupling. Nat Commun 12(1):4894. https://doi.org/10.1038/s41467-021-25184-4
15. Amico E, Goñi J (2018) Mapping hybrid functional-structural connectivity traits in the human connectome. Netw Neurosci (Cambridge Mass) 2(3):306–322. https://doi.org/10.1162/netn_a_00049
16. Valk SL, Xu T, Paquola C et al (2022) Genetic and phylogenetic uncoupling of structure and function in human transmodal cortex. Nat Commun 13(1):2341. https://doi:10.1038/s41467-022-29886-1
17. Baum GL, Cui Z, Roalf DR, Ciric R, Betzel RF, Larsen B et al (2020) Development of structure-function coupling in human brain networks during youth. Proc Natl Acad Sci USA 117(1):771–778. https://doi.org/10.1073/pnas.1912034117
18. Sotiras A, Toledo JB, Gur RE, Gur RC, Satterthwaite TD, Davatzikos C (2017) Patterns of coordinated cortical remodeling during adolescence and their associations with functional specialization and evolutionary expansion. Proc Natl Acad Sci USA 114(13):3527–3532. https://doi.org/10.1073/pnas.1620928114
19. Abdelnour F, Voss HU, Raj A (2014) Network diffusion accurately models the relationship between structural and functional brain connectivity networks. NeuroImage 90:335–347.

https://doi.org/10.1016/j.neuroimage.2013.12.039

20. Vázquez-Rodríguez B, Suárez LE, Markello RD, Shafiei G, Paquola C, Hagmann P et al (2019) Gradients of structure-function tethering across neocortex. Proc Natl Acad Sci USA 116(42):21219–21227. https://doi.org/10.1073/pnas.1903403116
21. Sanz Leon P, Knock SA, Woodman MM, Domide L, Mersmann J, McIntosh AR et al (2013) The Virtual Brain: a simulator of primate brain network dynamics. Front neuroinformatics 7:10. https://doi.org/10.3389/fninf.2013.00010
22. Greicius MD, Supekar K, Menon V, Dougherty RF (1991) Resting-state functional connectivity reflects structural connectivity in the default mode network. Cerebral cortex (New York, NY: 2009;19(1):72 – 8. https://doi.org/10.1093/cercor/bhn059
23. Horn A, Ostwald D, Reisert M, Blankenburg F (2014) The structural-functional connectome and the default mode network of the human brain. NeuroImage. https://doi.org/10.1016/j.neuroimage.2013.09.069. 102 Pt 1:142 – 51
24. Hall CN, Howarth C, Kurth-Nelson Z, Mishra A (2016) Interpreting BOLD: towards a dialogue between cognitive and cellular neuroscience. Philos Trans R Soc Lond B Biol Sci 371(1705):20150348. https://doi:10.1098/rstb.2015.0348
25. Siasios I, Kapsalaki EZ, Fountas KN, Fotiadou A, Dorsch A, Vakharia K et al (2016) The role of diffusion tensor imaging and fractional anisotropy in the evaluation of patients with idiopathic normal pressure hydrocephalus: a literature review. NeuroSurg Focus 41(3):E12. https://doi.org/10.3171/2016.6.FOCUS16192
26. Wang ML, Wei XE, Yu MM, Li WB (2022) Cognitive impairment in mild traumatic brain injury: a diffusion kurtosis imaging and volumetric study. Acta Radiol 63(4):504–512. https://doi:10.1177/0284185121998317
27. Struyfs H, Van Hecke W, Veraart J et al (2015) Diffusion Kurtosis Imaging: A Possible MRI Biomarker for AD Diagnosis? J Alzheimers Dis 48(4):937–948. https://doi:10.3233/JAD-150253
28. Friston KJ, Williams S, Howard R, Frackowiak RS, Turner R (1996) Movement-related effects in fMRI time-series. Magn Reson Med 35(3):346–355. https://doi:10.1002/mrm.1910 350312
29. Zhang HY, Chen WX, Jiao Y, Xu Y, Zhang XR, Wu JT (2014) Selective vulnerability related to aging in large-scale resting brain networks. PLoS ONE 9(10):e108807 Published 2014 Oct 1. https://doi:10.1371/journal.pone.0108807
30. Andrews-Hanna JR, Snyder AZ, Vincent JL, Lustig C, Head D, Raichle ME et al (2007) Disruption of large-scale brain systems in advanced aging. Neuron 56(5):924–935. https://doi.org/10.1016/j.neuron.2007.10.038
31. Tabesh A, Jensen JH, Ardekani BA, Helpern JA (2011) Estimation of tensors and tensor-derived measures in diffusional kurtosis imaging. Magn Reson Med 65(3):823–836. https://doi.org/10.1002/mrm.22655
32. Park HJ, Friston K (2013) Structural and functional brain networks: from connections to cognition. Sci (New York NY) 342(6158):1238411. https://doi.org/10.1126/science.1238411

33. Su H, Zhang L, Qiao L, Liu M (2022) Estimating high-order brain functional networks by correlation-preserving embedding. Med Biol Eng Comput 60(10):2813–2823. https://doi.org/10.1007/s11517-022-02628-7
34. Nieuwenhuys R, Broere CA (2017) A map of the human neocortex showing the estimated overall myelin content of the individual architectonic areas based on the studies of Adolf Hopf. Brain Struct function 222(1):465–480. https://doi.org/10.1007/s00429-016-1228-7
35. Fatterpekar GM, Naidich TP, Delman BN, Aguinaldo JG, Gultekin SH, Sherwood CC et al (2002) Cytoarchitecture of the human cerebral cortex: MR microscopy of excised specimens at 9.4 Tesla. AJNR Am J Neuroradiol 23(8):1313–1321
36. Die Cytoarchitektonik der Hirnrinde des erwachsenen Menschen (1926) (The Cyto-Architectonics of the Cerebral Cortex of Adult Man). Archives Neurol Psychiatry 16(6):816–816
37. Cohen-Adad J, Polimeni JR, Helmer KG, Benner T, McNab JA, Wald LL et al (2012) T_2* mapping and B_0 orientation-dependence at 7 T reveal cyto- and myeloarchitecture organization of the human cortex. NeuroImage 60(2):1006–1014. https://doi.org/10.1016/j.neuroimage.2012.01.053
38. Colón-Ramos DA (2009) Synapse formation in developing neural circuits. Curr Top Dev Biol 87:53–79. https://doi.org/10.1016/S0070-2153(09)01202-2
39. Barres BA (2008) The mystery and magic of glia: a perspective on their roles in health and disease. Neuron 60(3):430–440. https://doi.org/10.1016/j.neuron.2008.10.013
40. Liu X, Zhang Y, Chen F et al (2023) Preliminary research of the classification of the brain acute stroke lesions by the Diffusion Kurtosis Imaging (DKI) and Diffusion Weighted Imaging (DWI) parameters. Technol Health Care 31(S1):525–532. https://doi:10.3233/THC-236046
41. Hori M, Fukunaga I, Masutani Y et al (2012) Visualizing non-Gaussian diffusion: clinical application of q-space imaging and diffusional kurtosis imaging of the brain and spine. Magn Reson Med Sci 11(4):221–233. https://doi:10.2463/mrms.11.221
42. Guglielmetti C, Veraart J, Roelant E et al (2016) Diffusion kurtosis imaging probes cortical alterations and white matter pathology following cuprizone induced demyelination and spontaneous remyelination. NeuroImage 125:363–377. https://doi:10.1016/j.neuroimage.2015.10.052
43. Praet J, Manyakov NV, Muchene L et al (2018) Diffusion kurtosis imaging allows the early detection and longitudinal follow-up of amyloid-β-induced pathology. Alzheimers Res Ther 10(1):1 Published 2018 Jan 9. https://doi:10.1186/s13195-017-0329-8
44. Zhu T, Peng Q, Ouyang A, Huang H (2021) Neuroanatomical underpinning of diffusion kurtosis measurements in the cerebral cortex of healthy macaque brains. Magn Reson Med 85(4):1895–1908. https://doi:10.1002/mrm.28548
45. Helenius J, Soinne L, Perkiö J et al (2002) Diffusion-weighted MR imaging in normal human brains in various age groups. AJNR Am J Neuroradiol 23(2):194–199
46. Bremer B, Wu Q, Mora Álvarez MG et al Mindfulness meditation increases default mode, salience, and central executive network connectivity. Sci Rep, *12*(1), 13219. https://doi.org/10.1038/s41598-022-17325-6

47. Hugdahl K, Kazimierczak K, Beresniewicz J, Kompus K, Westerhausen R, Ersland L et al (2019) Dynamic up- and down-regulation of the default (DMN) and extrinsic (EMN) mode networks during alternating task-on and task-off periods. PLoS ONE 14(9):e0218358. https://doi.org/10.1371/journal.pone.0218358
48. Christoff K, Gordon AM, Smallwood J, Smith R, Schooler JW (2009) Experience sampling during fMRI reveals default network and executive system contributions to mind wandering. Proc Natl Acad Sci USA 106(21):8719–8724. https://doi.org/10.1073/pnas.0900234106
49. Gerlach KD, Spreng RN, Gilmore AW, Schacter DL (2011) Solving future problems: default network and executive activity associated with goal-directed mental simulations.Neuroimage.;55(4):1816-24. https://doi.org/10.1016/j.neuroi mage. 2011. 01.030
50. Chong JSX, Ng GJP, Lee SC, Zhou J (2017) Salience network connectivity in the insula is associated with individual differences in interoceptive accuracy. Brain Struct function 222(4):1635–1644. https://doi.org/10.1007/s00429-016-1297-7
51. Seeley WW (2019) The Salience Network: A Neural System for Perceiving and Responding to Homeostatic Demands. J neuroscience: official J Soc Neurosci 39(50):9878–9882. https://doi.org/10.1523/JNEUROSCI.1138-17.2019
52. Fransson P, Skiöld B, Horsch S, Nordell A, Blennow M, Lagercrantz H et al (2007) Resting-state networks in the infant brain. Proc Natl Acad Sci USA 104(39):15531–15536. https://doi.org/10.1073/pnas.0704380104
53. Fransson P, Skiöld B, Engström M et al (2009) Spontaneous brain activity in the newborn brain during natural sleep–an fMRI study in infants born at full term. Pediatr Res 66(3):301–305. https://doi.org/10.1203/PDR.0b013e3181b1bd84
54. Adams RA, Shipp S, Friston KJ (2013) Predictions not commands: active inference in the motor system. Brain Struct function 218(3):611–643. https://doi.org/10.1007/s00429-012-0475-5
55. Ossmy O, Mukamel R (2018) Behavioral and neural effects of congruency of visual feedback during short-term motor learning. NeuroImage. https://doi.org/10.1016/j.neuroimage.2017.12.020. 172:864 – 73
56. Mukherjee P, Miller JH, Shimony JS et al (2002) Diffusion-tensor MR imaging of gray and white matter development during normal human brain maturation. AJNR Am J Neuroradiol 23(9):1445–1456

Figures

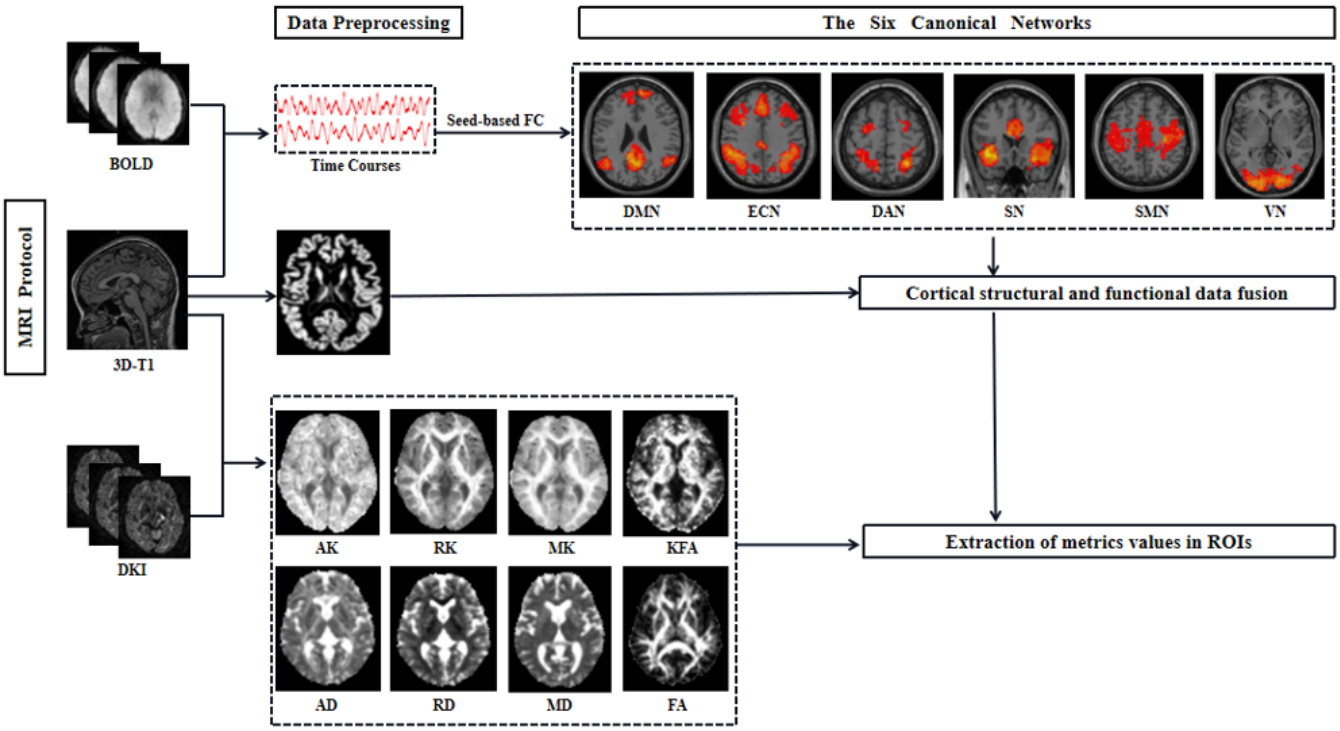


Figure 1

Overview of the measurement scheme for data processing.

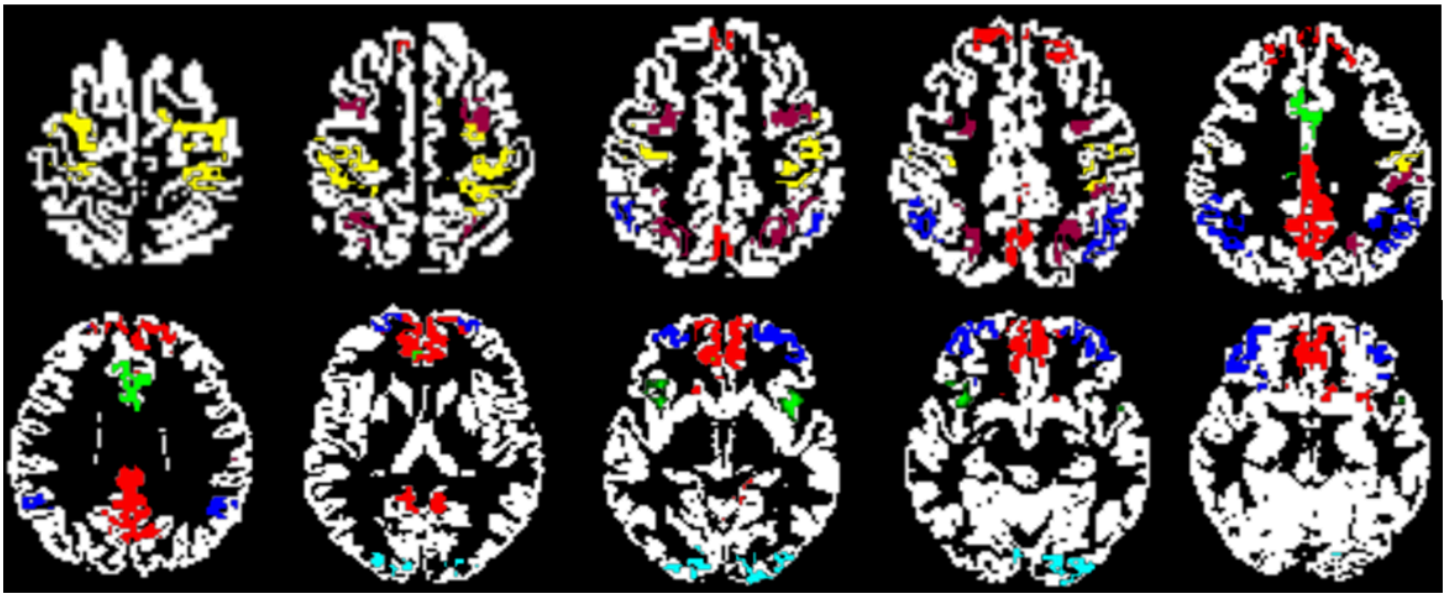


Figure 2

Projection of the six canonical networks mere on the cortex. The six canonical networks were precisely immerged only into the segmented cortical areas in each individual to avoid the subcortical white matter

interference. Yellow color represents the SMN; Purple color represents the DAN; Red color represents the DMN; Blue color represents the ECN; Green color represents the SN; Cool blue color represents the VN.

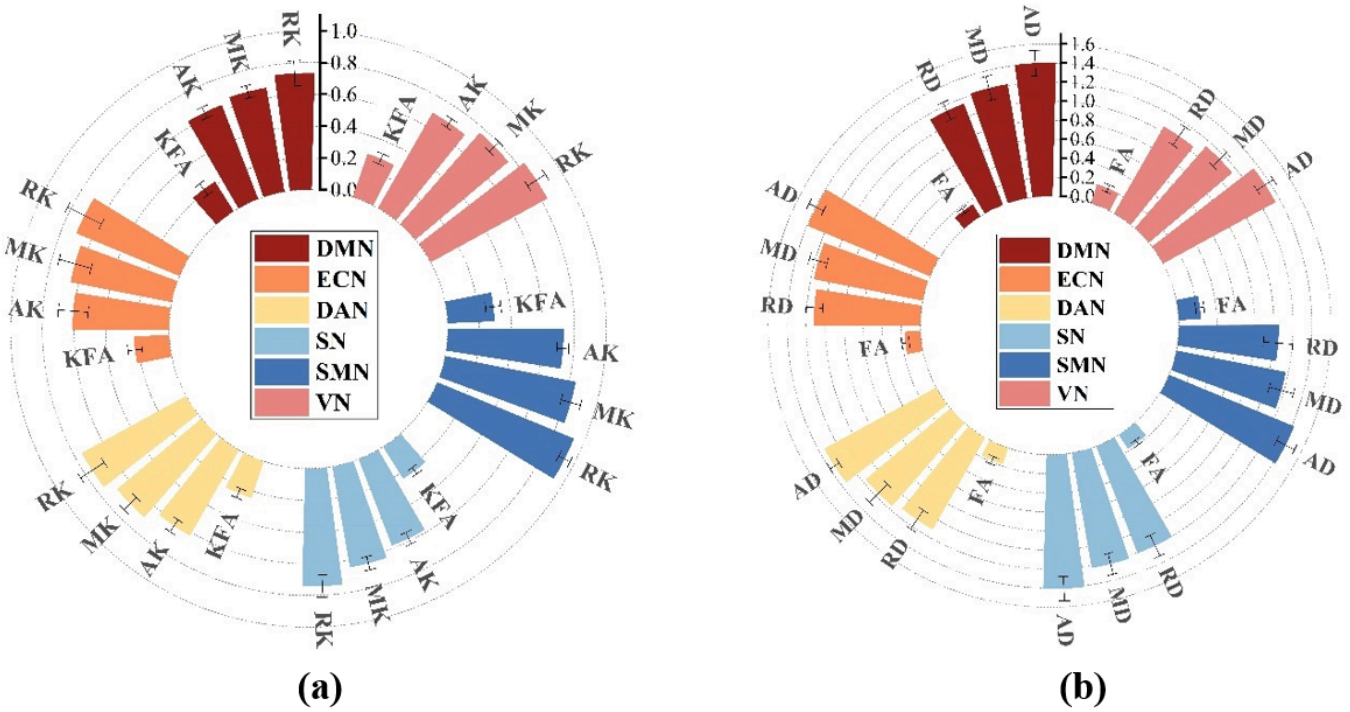


Figure 3

the distribution of DK and DT metric value sizes in the cortical regions of the six canonical brain networks, represented by (a) and (b) respectively. The histogram represents the range of the diffusion metric values for each of the canonical functional networks(means ± standard deviation).

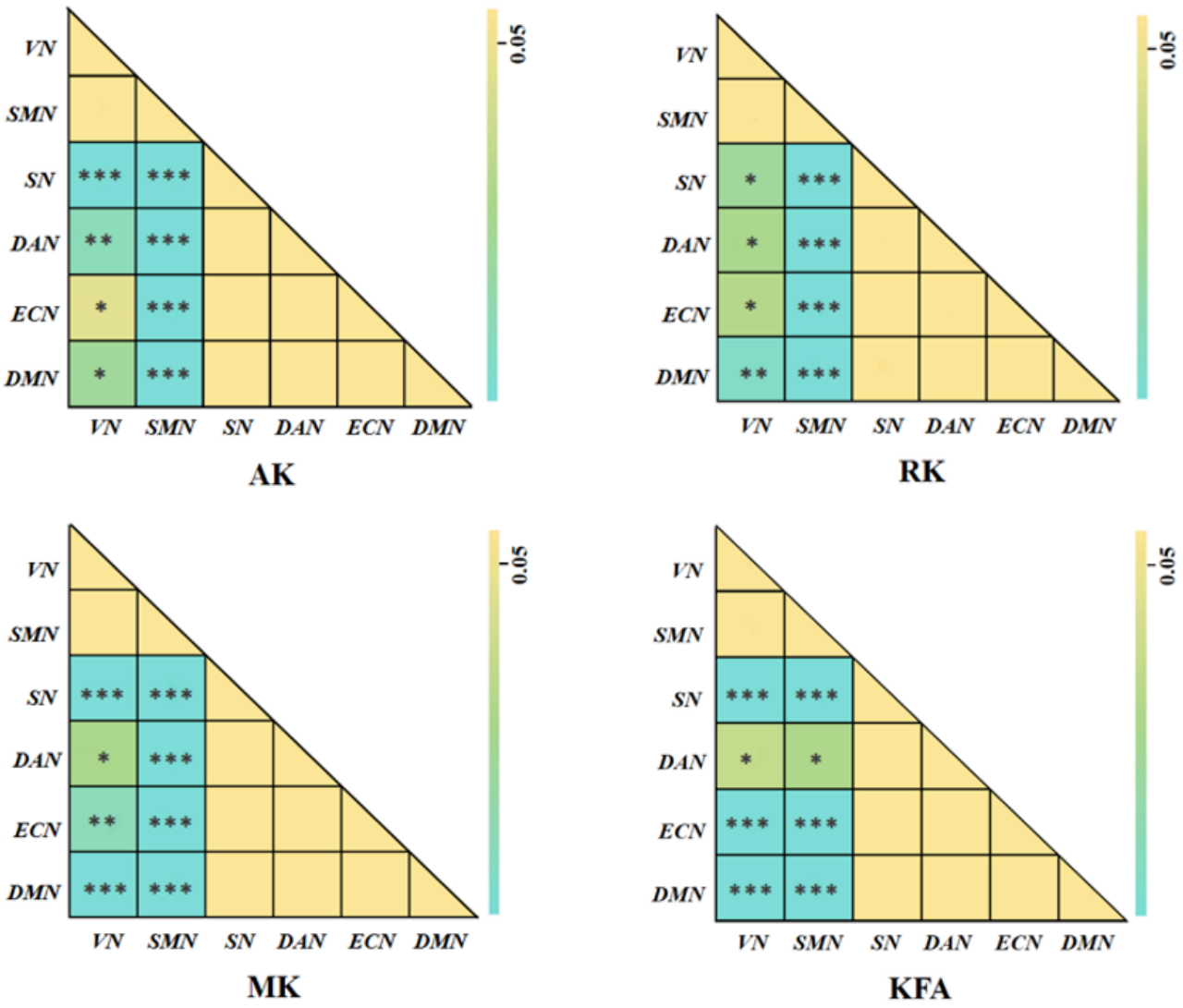


Figure 4

The comparison for each DK metrics in the six canonical networks cortical areas. DMN: default mode network; ECN: executive control network; DAN: dorsal attention network; SN: salience network; SMN: sensorimotor network; VN: visual network. AK: axial kurtosis; RK: radial kurtosis; MK: mean kurtosis; KFA: kurtosis fractional anisotropy. The color bar denotes the P value. The statistical threshold was set at $p<0.05$ with Kruskal-Wallis H test and was corrected with Bonferroni method. ▯▯▯ represents $p<0.001$, ▯▯ represents $p<0.01$, ▯ represents $p<0.05$.

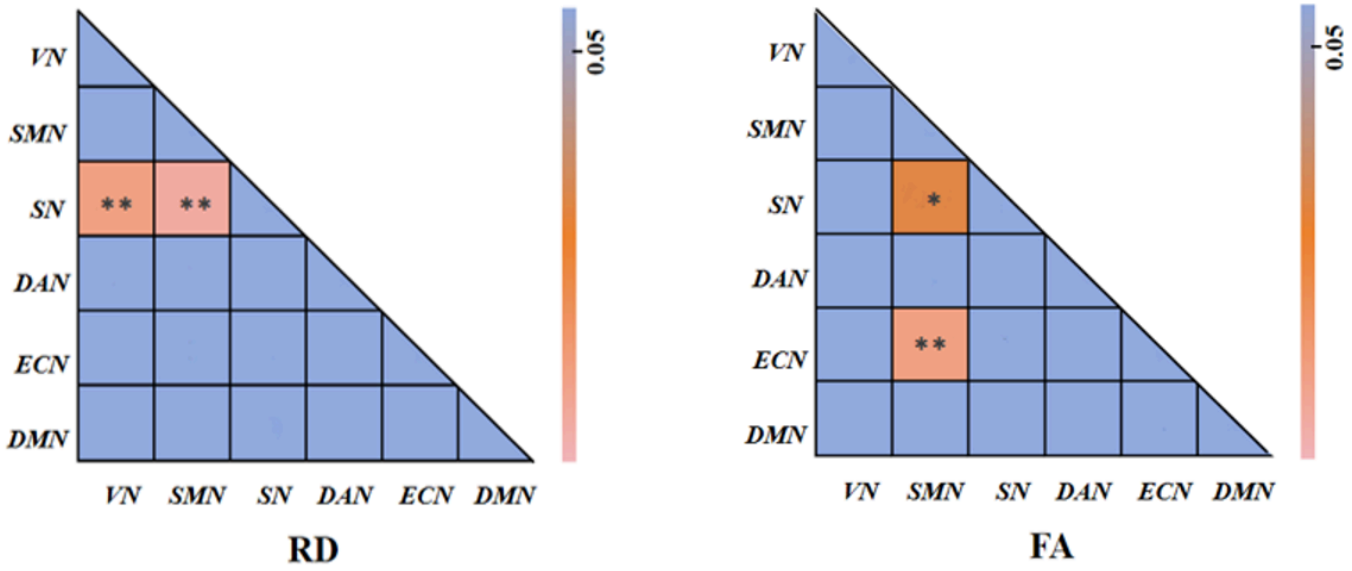


Figure 5

The comparison for RD and FA of DT metrics in the six canonical networks cortical areas. DMN: default mode network; ECN: executive control network; DAN: dorsal attention network; SN: salience network; SMN: sensorimotor network; VN: visual network. RD: radial diffusivity; FA: fractional anisotropy. The color bar denotes the P value. The statistical threshold was set at $p<0.05$ with Kruskal-Wallis H test and was corrected with Bonferroni method. ** represents $p<0.01$, * represents $p<0.05$.